RSC Advances

RSC Publishing

PAPER

View Article Online
View Journal | View Issue

Cite this: *RSC Adv.*, 2013, **3**, 20613

High-performance flexible solid-state supercapacitors based on MnO_2-decorated nanocarbon electrodes

Yang Gao,[a] Yun Shen Zhou,[a] Min Qian,[b] Hao Ming Li,[c] Jody Redepenning,[c] Li Sha Fan,[a] Xiang Nan He,[a] Wei Xiong,[a] Xi Huang,[a] Masoud Majhouri-Samani,[a] Lan Jiang[d] and Yong Feng Lu*[a]

Received 18th June 2013
Accepted 29th August 2013

DOI: 10.1039/c3ra43039a

www.rsc.org/advances

Flexible energy storage units are highly desired to meet the ever-increasing demands for flexible electronics. In this paper, highly flexible solid-state supercapacitors are fabricated using MnO_2-decorated nanocarbon electrodes and 1-ethyl-3-methylimidazolium bis(trifluoromethylsulfonyl)imide–poly(vinylidene fluoride)-hexafluoropropylene ([EMIM][NTf2]–PVdF(HFP)) gel electrolytes. The flexible electrodes are prepared by electrodepositing MnO_2 onto the carbon nanotube/carbon nanoonion (CNT/CNO) films. CNT/CNO films have a large surface area for MnO_2 deposition and work as mechanical supports with high flexibility and light weight. CNOs act as spacers to separate CNTs, introducing mesopores inside the CNT/CNO films for preventing pore blocking during MnO_2 deposition. The supercapacitor exhibits enhanced electrochemical performance with an energy density of 16.4 W h^{-1} kg^{-1} at a power density of 33.3 kW kg^{-1} by using the [EMIM][NTf2]–PVdF(HFP) gel electrolyte. Moreover, the supercapacitors can exhibit high electrochemical performance under large mechanical stress, making the devices suitable for flexible electronics.

1. Introduction

The ever-increasing demands for flexible, portable electronics[1–8] are driving research on flexible energy conversion and storage units.[9–13] As some of the major energy storage devices, supercapacitors have been widely used in high-power applications[14–17] because of their higher energy density than dielectric capacitors and higher power density, longer cycle life than batteries.[18–23] Nevertheless, the conventional supercapacitors use rigid packages which are not applicable in flexible electronics.[24] In addition, the liquid electrolyte has leakage risks.[24,25] Therefore, high-performance flexible solid-state supercapacitors are highly desired to meet requirements in the future flexible electronics.

Supercapacitors can be classified into two types, electrical double-layer capacitors and pseudocapacitors, in terms of charge storage mechanisms.[26] Carbon materials[16,27] are promising electrode materials for electrical double-layer capacitors, which have high power density and long cycle life but suffer from relatively low capacitance. Transition metal oxides have been studied as pseudocapacitor electrodes because of their much higher capacitances as compared to carbon materials. Among them, manganese oxides have been studied extensively due to the low cost, abundance, and environmental friendliness.[26–29]

To develop flexible solid-state supercapacitors based on manganese oxide/carbon hybrid structures can fully utilize both advantages of double-layer and pseudocapacitances to achieve enhanced energy and power densities. Up to now, a number of flexible manganese oxide/carbon hybrid structures have been investigated for supercapacitors by depositing manganese oxides onto various carbon materials.[26,28–31] In those studies, however, the electrochemical performance of manganese oxide/carbon hybrid electrodes was not studied for nonliquid electrolytes, which are more suitable for flexible and solid-state devices. Recently, Yuan *et al.* have fabricated flexible solid-state supercapacitors based on MnO_2/carbon hybrid electrodes and phosphoric acid–polyvinyl alcohol (H_3PO_4–PVA) gel electrolyte, which provide an energy density of 4.8 W h^{-1} kg^{-1}.[25] Nevertheless, due to the limited electrochemical potential window of the H_3PO_4–PVA gel electrolyte (~1 V), further efforts are required to improve the energy density of the solid-state devices. As a class of promising electrolytes, ionic liquids have attracted attention due to their high ion conductivity, nonvolatility, high thermal stability, and broad electrochemical potential windows (as high as 3–3.5 V).[32] Investigations have been conducted to evaluate the application of ionic liquids in manganese oxide based supercapacitors.[33,34] It is suggested that the charge storage mechanism of MnO_2 in ionic liquid is mainly ascribed to anion insertion/deinsertion process, which compensates the Mn valent state change.[33,34]

[a]*Department of Electrical Engineering, University of Nebraska-Lincoln, Lincoln, NE 68588-0511, USA. E-mail: ylu2@unl.edu; Tel: +1-402-472-8323*

[b]*Department of Chemistry, University of Nebraska-Lincoln, 534 HAH, Lincoln, NE 68588-0304, USA*

[c]*Department of Physics, East China Normal University, Shanghai, 200062, China*

[d]*Department of Mechanical and Automation Engineering, Beijing Institute of Technology, Beijing, 10008, China*

In this work, flexible solid-state supercapacitors were fabricated using MnO_2-decorated nanocarbon electrodes and 1-ethyl-3-methylimidazolium bis(trifluoromethylsulfonyl)imide–poly (vinylidene fluoride)-hexafluoropropylene ([EMIM][NTf2]–PVdF(HFP)) gel electrolyte. The porous carbon nanotube/carbon nanoonion (CNT/CNO) films work as a flexible, lightweight matrix for hosting MnO_2. [EMIM][NTf2]–PVdF(HFP) gel electrolyte was used to avoid the requirements of rigid packages.[35] The flexible solid-state supercapacitors assembled using the MnO_2-decorated nanocarbon electrodes and [EMIM][NTf2]–PVdF(HFP) gel electrolyte provide the highest energy density of 16.4 W h^{-1} kg^{-1} at a power density of 33.3 kW kg^{-1}. Moreover, the devices can maintain high electrochemical performance under large mechanical stress and hence are suitable for flexible electronics.

2. Experimental section

2.1 Preparation of the CNT/CNO films

CNT/CNO films were prepared by vacuum filtration of a CNT/CNO solution using porous mixed cellulose ester (MCE) membranes (0.45 μm, 47 mm in diameter). CNTs with a specific surface area (SSA) of 407 m^2 g^{-1} from Cheaptubes, Inc. were used. CNOs having an SSA of 450 m^2 g^{-1} were synthesized by a laser-assisted combustion process.[36] CNTs and CNOs at a weight ratio of 1 : 1 were dispersed in deionized (DI) water using sodium dodecylbenzenesulfonate as a surfactant. CNT/CNO films were prepared by filtration of the solution through porous MCE membranes and drying at room temperature for 2 h. The deposited CNT/CNO films were placed on adhesive tapes and treated with acetone vapor for 2 min to make the MCE membranes transparent and highly flexible.[37] After removal of the tape, the resulting flexible CNT/CNO films were cut to the desired size for electrodeposition of manganese dioxide (MnO_2).

2.2 Electrodeposition of MnO_2 onto the CNT/CNO films

Electrodeposition of MnO_2 was carried out in an aqueous solution of 0.02 M $MnSO_4 \cdot H_2O$ and 0.2 M Na_2SO_4 using chronoamperometry.[28] The CNT/CNO films, platinum foil, and a Ag/AgCl wire were used as the working, counter, and reference electrodes, respectively. The applied potential is ~0.9 V. The time for electrodeposition of MnO_2 on CNT/CNO films was from 1 to 15 min.

2.3 Fabrication of flexible solid-state supercapacitors

The flexible solid-state supercapacitors were fabricated using the MnO_2/CNT/CNO electrodes and the [EMIM][NTf2]–PVdF(HFP) gel electrolyte in a glove box under an atmosphere of nitrogen. The [EMIM][NTf2]–PVdF(HFP) gel electrolyte was prepared as follows:[38] a mixture of [EMIM][NTf2] and PVDF-*co*-HFP (mass ratio 2 : 1) was dissolved in a 15 ml 4-methyl-2-pentanone. The mixture was heated to 100 °C by stirring for 30 min. A small amount of [EMIM][NTf2]–PVdF(HFP) was cast onto two pieces of the MnO_2/CNT/CNO electrodes. Then the two electrodes were assembled together with cellulose paper as a separator. The device was then put into a fume hood for solidifying the [EMIM][NTf2]–PVdF(HFP) gel electrolyte.[38]

2.4 Characterization

A field-emission scanning electron microscope (Hitachi S4700 FE-SEM system, maximum resolution of 1.2 nm at 25 kV) was used to study the morphology of the electrodes. A Renishaw inVia dispersive micro-Raman spectrometer with a 514 nm excitation source was used for Raman spectroscopic study. A standard 50× objective was used for the Raman characterizations, which provided a focal spot diameter of ~2 μm. The XRD patterns were obtained with a Bruker-AXS D8 Discover High-Resolution diffractometer using Cu Kα radiation.

The electrochemical investigation of the flexible solid-state supercapacitors was conducted on a CHI 760D (Shanghai Chenhua, China) electrochemical workstation.

The capacitance of supercapacitors from a cyclic voltammogram (CV) was given by:

$$C = \frac{\int \frac{i\mathrm{d}V}{m}}{v\Delta V}, \quad (1)$$

where i is the response current, ΔV is the potential range of CV, v is the potential scan rate, respectively. m is the mass for the MnO_2/CNT/CNO electrodes.

Additionally, capacitance from galvanostatic charge–discharge (GCD) was calculated using the following formula:

$$C = \frac{i}{m(\mathrm{d}V/\mathrm{d}t)}, \quad (2)$$

where i is the constant current, and $\mathrm{d}V/\mathrm{d}t$ is the slope of the discharge curve.

The energy density of the supercapacitors was estimated by:

$$E = \frac{C(\Delta U)^2}{2}, \quad (3)$$

where ΔU is the discharge potential after the iR drop.

The power density of the supercapacitors was given by:

$$P = \frac{\Delta U^2}{4R}. \quad (4)$$

3. Results and discussion

CNT/CNO films were prepared by vacuum filtration of CNT/CNO solution using porous mixed cellulose esters (MCE) membranes. Fig. 1a shows a photograph of a typical CNT/CNO film, which is highly flexible. The sheet resistance of the CNT/CNO is ~30 Ω $\square^{-1}$. Fig. 1b shows a scanning electron microscope (SEM) image of the CNT/CNO films. In contrast to the CNT films (Fig. 1c), in which CNTs are densely entangled, CNT/CNO films use CNOs as spacers to separate CNTs and introduce more mesopores inside the CNT/CNO films. For electrodeposition of functional materials, mesopores can reduce pore blocking during the deposition process.[20,26] The CNT/CNO films with large SSA and high conductivity were used as the backbone for the electrodeposition of MnO_2. The electrodeposition of MnO_2 was conducted in a solution containing 0.02 M $MnSO_4$ and 0.2 M Na_2SO_4. Fig. 2a–d shows the morphologies of CNT/CNO films with MnO_2 deposition for different times. By

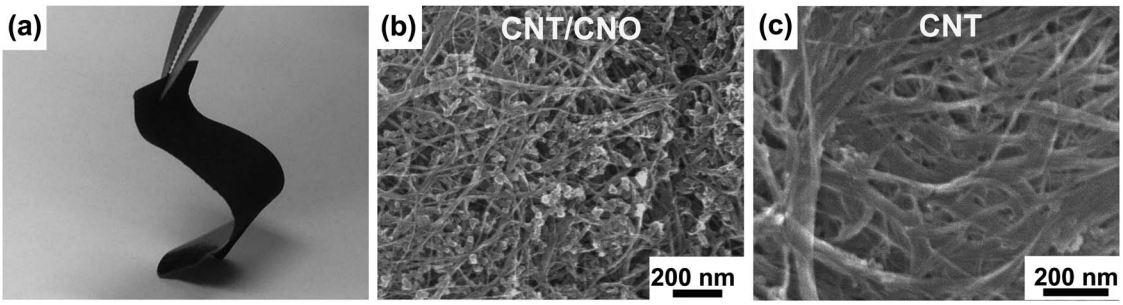

Fig. 1 (a) A photograph of a typical flexible CNT/CNO composite film. (b) SEM micrograph of the CNT/CNO composite film. (c) SEM micrograph of a CNT film.

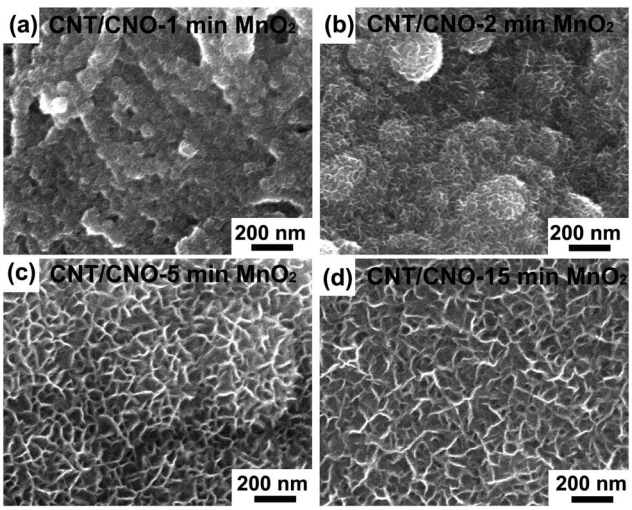

Fig. 2 (a–d) SEM images of CNT/CNO films with MnO_2 deposition for 1, 2, 5, and 15 min.

increasing the deposition time, more MnO_2 is deposited on the CNT/CNO films. For a deposition time of 1 min, a thin layer of MnO_2 is coated on the surface of the CNT/CNO film, as shown in Fig. 2a. The MnO_2 layer deposited is not well connected, as indicated by the pores shown in Fig. 2a. By increasing the deposition time to 2 min, a continuous MnO_2 film is formed on the surface of the CNT/CNO film (Fig. 2b). The continuous MnO_2 film prevents Mn ions from penetrating and reaching the CNT/CNO film which would stop the growth of MnO_2 on the CNT/CNO backbone.[28] Further increase in the deposition time leads to a thickness increase in the MnO_2 films (Fig. 2c and d), which increases the ion transportation path and slows down the faradaic redox reactions.[26]

Fig. 3a shows the Raman spectra of the MnO_2/CNT/CNO electrodes synthesized by electrodeposition of MnO_2 onto the CNT/CNO films. Three bands, located at 507, 561, and 643 cm^{-1}, are ascribed to MnO_2.[28,39,40] The bands ranging from 100 to 300 cm^{-1} are ascribed to the radial breathing modes of the CNTs.[41] As shown in Fig. 3a, the intensities of radial breathing modes of the CNTs decrease with an increase in the deposition time. The Raman band signals for MnO_2 increase with increasing deposition time. For a deposition of 1 min, only a broad band ranging from 400 to 700 cm^{-1} is observed, indicating poor crystallinity of the MnO_2 deposited. With deposition times longer than 2 min, Raman bands for MnO_2 are clearly observed. Those observations indicate that the film thickness increases with longer deposition time (Fig. 2a–d). Fig. 3b shows the X-ray diffraction (XRD) patterns of the MnO_2/CNT/CNO electrodes. For the samples with a deposition time of less than 5 min, the carbon materials show XRD peaks at only 11° and 20°. The MnO_2/CNT/CNO electrodes prepared by 5 to 15 min depositions show weak peaks at 37° and 66°. All of these findings suggest the amorphous nature of the MnO_2 films.[28,42]

To realize flexible solid-state supercapacitors, the MnO_2/CNT/CNO electrodes and [EMIM][NTf2]–PVdF(HFP) gel electrolyte were used for device fabrication. Fig. 4a shows a

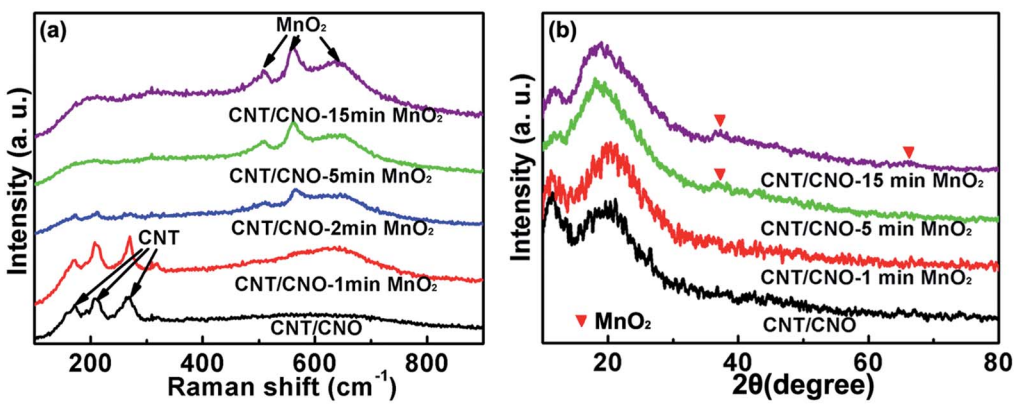

Fig. 3 (a) Raman spectra and (b) XRD patterns of the as-synthesized MnO_2/CNT/CNO electrodes.

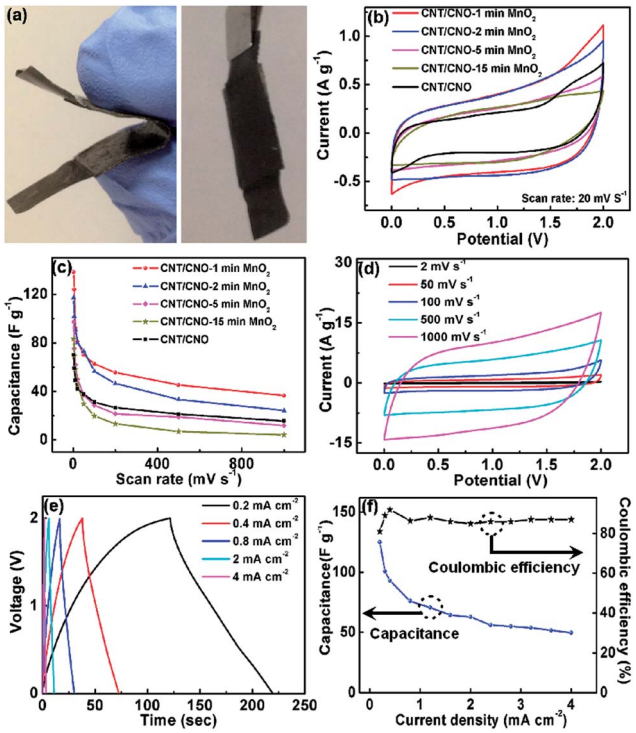

Fig. 4 (a) Photographs of the solid-state supercapacitor fabricated by 1 min MnO_2/CNT/CNO electrodes. (b) CV curves of the solid-state supercapacitors fabricated by the hybrid electrodes with various MnO_2 deposition time at a potential scan rate of 20 mV s^{-1}. (c) The capacitance of the solid-state supercapacitors as a function of the scan rate. (d) CV curves of the supercapacitor fabricated by 1 min MnO_2/CNT/CNO electrodes at scan rates from 2 to 1000 mV s^{-1}. (c) GCD curves for the supercapacitor (1 min MnO_2 deposition) at different current densities from 0.2 to 4 mA cm^{-2}. (d) Capacitance and coulombic efficiency of the supercapacitor (1 min MnO_2 deposition) as function of the current density.

photograph of a supercapacitor fabricated by the 1 min MnO_2/CNT/CNO electrodes and gel electrolyte. The device is thin and flexible. The thickness of the supercapacitor is approximately 120 μm. For an electrode with the size of 1 × 1 cm^2, the mass loading of CNT, CNO, and MnO_2 is ~0.4 mg. The electrochemical behaviors of the supercapacitors fabricated by the hybrid electrodes with various MnO_2 deposition time were studied by CV and GCD measurements. Fig. 4b shows the CV curves of the supercapacitors at a scan rate of 20 mV s^{-1}. The CV curves of the supercapacitors fabricated by 1- and 2-min MnO_2/CNT/CNO electrodes demonstrate the rectangular symmetry, indicating facile charging and discharging characteristics. However, the supercapacitors based on electrodes with 15 min MnO_2 deposition lost the rectangular symmetry in the CV curves due to the high ion transportation resistances caused by the densely deposited MnO_2 on the CNT/CNO films.[26] Fig. 4c shows the capacitance of the supercapacitors as a function of the scan rate. The supercapacitor (1 min MnO_2 deposition) demonstrates the highest capacitance at all scan rates. At 2 mV s^{-1}, the capacitance is 138 F g^{-1} (51 mF cm^{-2} and 4.25 F cm^{-3}). Fig. 4d shows CV curves for the supercapacitor prepared by 1 min MnO_2/CNT/CNO electrodes recorded at scan rates from 2 to 1000 mV s^{-1}. With increased scan rates up to 1000 mV s^{-1}, the CV curves still maintained rectangular symmetry, which is ascribed to the highly conductive CNT/CNO film and the thin MnO_2 layer with low ion transportation resistance.[26] Fig. 4e shows the GCD curves of the supercapacitor (1 min MnO_2 deposition) at different current densities from 0.2 to 4 mA cm^{-2}. The capacitance of the device decreases from 125 F g^{-1} (50 mF cm^{-2}) to 50 F g^{-1} (20 mF cm^{-2}) (Fig. 4f) as the current density increases from 0.2 to 4 mA cm^{-2}, corresponding to about 40% capacitance retention. The coulombic efficiency of the supercapacitor is close to 90% in the current density range, indicating a stable electrochemical performance of the supercapacitor.[43] The MnO_2/CNT/CNO based solid-state supercapacitor has higher specific capacitance than previously reported solid-state devices fabricated by CNT,[21,44] graphene,[26,45] and MnO_2/carbon hybrid electrodes.[25] Despite of lower capacitance in contrast to recently reported solid-state devices based on graphene hydrogel,[46] MnO_2/graphene,[47] and vanadium nitride nanowire,[48] the supercapacitors using MnO_2/CNT/CNO electrodes provide higher or comparable energy densities due to the use of ionic liquid based gel electrolyte (Fig. 6b).

To demonstrate the device capability for flexible energy storage, the electrochemical performance of the supercapacitor

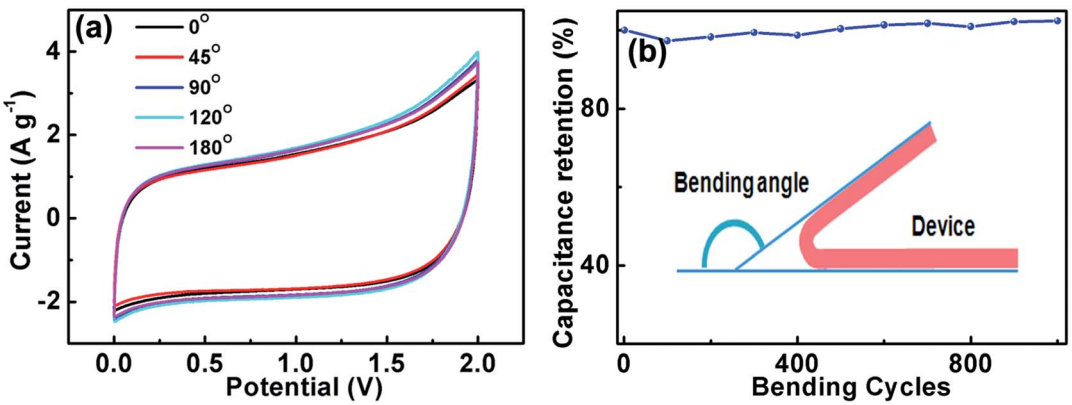

Fig. 5 (a) Cyclic voltammetry curves for the supercapacitor at different bending angles from 0–180°. (b) Stability of the device during 1000 bending cycles (bending angle: 120°).

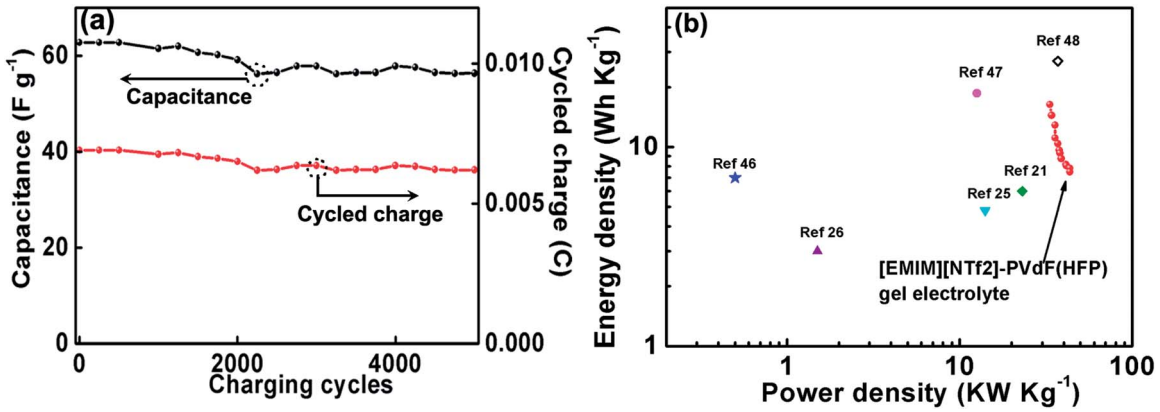

Fig. 6 (a) Retention ratio of the supercapacitor fabricated by 1 min MnO_2/CNT/CNO electrodes and [EMIM][NTf2]–PVdF(HFP) gel electrolyte in 5000 charge–discharge cycles at a current density of 2 mA cm^{-2}. (b) Ragone plots of the supercapacitors using [EMIM][NTf2]–PVdF(HFP) gel electrolytes.

fabricated by 1 min MnO_2/CNT/CNO electrodes under mechanical stress was investigated. Fig. 5a shows the CV performance of the device tested under different bending conditions at a scan rate of 100 mV s^{-1}. The device performance does not degrade under different bending conditions, which is ascribed to the mechanical flexibility of the MnO_2/CNT/CNO electrodes and [EMIM][NTf2]–PVdF(HFP) gel electrolyte. Moreover, in contrast to supercapacitors based on H_3PO_4–PVA gel electrolyte,[25] a larger electrochemical potential window (~2 V) is achieved for the supercapacitors using [EMIM][NTf2]–PVdF(HFP) gel electrolyte. The larger electrochemical potential window ensures a higher energy density. The stability and durability of the device was further investigated up to 1000 bending cycles, as shown in Fig. 5b. No obvious change in the electrochemical performance was observed, proving the high mechanical flexibility and stability of the devices.

The durability of supercapacitors fabricated by 1 min MnO_2/CNT/CNO electrodes and the [EMIM][NTf2]–PVdF(HFP) gel electrolyte was investigated through a cyclic charge–discharge process at a current density of 2 mA cm^{-2}, as shown in Fig. 6a. After 5000 charge–discharge cycles, approximately 90% of the initial capacitance (62.8 F g^{-1}) is preserved. A Ragone plot depicting energy density *versus* power density of the supercapacitors is shown in Fig. 6b. The supercapacitors using the [EMIM][NTf2]–PVdF(HFP) gel electrolyte achieve a maximum energy density of 16.4 W h^{-1} kg^{-1} at a power density of 33.3 kW kg^{-1}.

4. Conclusions

In this study, high-performance, flexible solid-state supercapacitors were successfully fabricated using MnO_2-decorated nanocarbon electrodes and [EMIM][NTf2]–PVdF(HFP) gel electrolyte. The supercapacitors are thin, lightweight, and highly flexible due to the mechanical flexibility of the composite electrodes and the gel electrolyte. The CNT/CNO films with high SSA and high mechanical flexibility act as the mechanical support for the MnO_2 deposition, ensuring high electrochemical performance and flexibility. Compared with traditional liquid electrolytes, the gel-electrolyte avoids a rigid package. The flexible solid-state supercapacitors achieve the highest energy density of 16.4 W h^{-1} kg^{-1} at a power density of 33.3 kW kg^{-1}. Furthermore, these devices can maintain high electrochemical stability under large mechanical stress and hence meet the requirements for flexible electronic devices.

Acknowledgements

The authors thank Dr Han Chen and Dr Shah Valloppilly at the University of Nebraska-Lincoln for SEM and XRD technical support. This research work was financially supported by the National Science Foundation (CMMI 0758199 and CMMI 1129613), Nebraska Center for Energy Science Research, and Office of Naval Research (N00014-09-1-0943).

Notes and references

1 L. Nyholm, G. Nyström, A. Mihranyan and M. Strømme, *Adv. Mater.*, 2011, **23**, 3751.
2 S. Liu, P. Wang, Q. Zhao, H. Yang, J. Wong, H. Sun, X. Dong and W. Lin, *Adv. Mater.*, 2012, **24**, 2901.
3 S. Ju, J. Li, J. Liu, P. C. Chen, Y. G. Ha, F. Ishikawa, H. Chang, C. Zhou, A. Facchetti, D. B. Janes and T. J. Marks, *Nano Lett.*, 2008, **8**, 997.
4 S. I. Park, Y. Xiong, R. H. Kim, P. Elvikis, M. Meitl, D. H. Kim, J. Wu, J. Yoon, C. J. Yu, Z. Liu, Y. Huang, K. C. Hwang, P. Ferreira, X. Li, K. Choquette and J. A. Rogers, *Science*, 2009, **325**, 977.
5 S. Ju, A. Facchetti, X. Xuan, J. Liu, F. Ishikawa, P. D. Ye, C. Zhou, T. J. Marks and D. B. Janes, *Nat. Nanotechnol.*, 2007, **2**, 378.
6 Q. Cao, S. H. Hur, Z. T. Zhu, Y. Sun, C. Wang, M. A. Meitl, M. Shim and J. A. Rogers, *Adv. Mater.*, 2006, **18**, 18304.
7 Z. Wu, Z. Chen, X. Du, J. M. Logan, J. Sippel, M. Nikolou, K. Kamaras, J. R. Reynolds, D. B. Tanner, A. F. Hebard and A. G. Rinzler, *Science*, 2004, **305**, 1273.
8 S. Bae, H. Kim, Y. Lee, X. Xu, J. S. Park, Y. Zheng, J. Balakrishnan, T. Lei, H. R. Kim, Y. I. Song, Y. J. Kim, K. S. Kim, B. Ozyilmaz, J. H. Ahn, B. H. Hong and S. Iijima, *Nat. Nanotechnol.*, 2010, **5**, 574.

9 S. D. Perera, B. Patel, N. Nijem, K. Roodenko, O. Seitz, J. P. Ferraris, Y. J. Chabal and K. J. Balkus, *Adv. Energy Mater.*, 2011, **1**, 936.
10 V. Presser, L. Zhang, J. J. Niu, J. McDonough, C. Perez, H. Fong and Y. Gogotsi, *Adv. Energy Mater.*, 2011, **1**, 423.
11 J. J. Yoo, K. Balakrishnan, J. Huang, V. Meunier, B. G. Sumpter, A. Srivastava, M. Conway, A. L. M. Reddy, J. Yu, R. Vajtai and P. M. Ajayan, *Nano Lett.*, 2011, **11**, 1423.
12 G. Guo, L. Huang, Q. Chang, L. Ji, Y. Liu, Y. Xie, W. Shi and N. Jia, *Appl. Phys. Lett.*, 2011, **99**, 083111.
13 J. Ge, G. Cheng and L. Chen, *Nanoscale*, 2011, **3**, 3084.
14 J. R. Miller and P. Simon, *Science*, 2008, **321**, 651.
15 L. Zhao, L. Z. Fan, M. Q. Zhou, H. Guan, S. Y. Qiao, M. Antonietti and M. M. Titirici, *Adv. Mater.*, 2010, **22**, 5202.
16 M. Inagakia, H. Konnoa and O. Tanaike, *J. Power Sources*, 2010, **195**, 7880.
17 P. Simon and Y. Gogotsi, *Nat. Mater.*, 2008, **7**, 845.
18 L. L. Zhang and X. S. Zhao, *Chem. Soc. Rev.*, 2009, **38**, 2520.
19 K. H. An, W. S. Kim, Y. S. Park, Y. C. Choi, S. M. Lee, D. C. Chung, D. J. Bae, S. C. Y. Lim and H. Lee, *Adv. Mater.*, 2001, **13**, 497.
20 A. Izadi-Najafabadi, T. Yamada, D. N. Futaba, M. Yudasaka, H. Takagi, H. Hatori, S. Iijima and K. Hata, *ACS Nano*, 2011, **5**, 811.
21 M. Kaempgen, C. K. Chan, J. Ma, Y. Cui and G. Gruner, *Nano Lett.*, 2009, **9**, 1872.
22 P. Li, X. Lim, Y. Zhu, T. Yu, C. K. Ong, Z. Shen, A. T. S. Wee and C. H. Sow, *J. Phys. Chem. B*, 2007, **111**, 1672.
23 A. Burke, *J. Power Sources*, 2000, **91**, 37.
24 C. Meng, C. Liu, L. Chen, C. Hu and S. Fan, *Nano Lett.*, 2010, **10**, 4025.
25 L. Yuan, X. H. Lu, X. Xiao, T. Zhai, J. Dai, F. Zhang, B. Hu, X. Wang, L. Gong, J. Chen, C. Hu, Y. Tong, J. Zhou and Z. L. Wang, *ACS Nano*, 2012, **6**, 656.
26 Y. H. Lin, T. Y. Wei, H. C. Chien and S. Y. Lu, *Adv. Energy Mater.*, 2011, **1**, 901.
27 C. D. Lokhande, D. P. Dubal and O. S. Joo, *Curr. Appl. Phys.*, 2011, **11**, 255.
28 J. H. Kim, K. H. Lee, L. J. Overzet and G. S. Lee, *Nano Lett.*, 2011, **11**, 2611.
29 C. Z. Yuan, B. Gao, L. F. Shen, S. D. Yang, L. Hao, X. J. Lu, F. Zhang, L. J. Zhang and X. G. Zhang, *Nanoscale*, 2011, **3**, 529.
30 Q. Cheng, J. Tang, J. Ma, H. Zhang, N. Shinya and L. C. Qin, *Carbon*, 2011, **49**, 2917.
31 G. R. Li, Z. P. Feng, Y. N. Ou, D. Wu, R. W. Fu and Y. X. Tong, *Langmuir*, 2010, **26**, 2209.
32 T. Y. Kim, H. W. Lee, M. Stoller, D. R. Dreyer, C. W. Bielawski, R. S. Ruoff and K. S. Suh, *ACS Nano*, 2011, **5**, 436.
33 J. K. Chang, M. T. Lee, C. W. Cheng, W. Ta Tsai, M. Jay Deng and I. W. Sun, *Electrochem. Solid-State Lett.*, 2009, **12**, A19.
34 P. J. Hall, M. Mirzaeian, S. I. Fletcher, F. B. Sillars, A. J. R. Rennie, G. O. Shitta-Bey, G. Wilson, A. Cruden and R. Carter, *Energy Environ. Sci.*, 2010, **3**, 1238.
35 M. F. El-Kady, V. Strong, S. Dubin and R. B. Kaner, *Science*, 2012, **335**, 1326.
36 Y. Gao, Y. S. Zhou, J. B. Park, H. Wang, X. N. He, H. F. Luo, L. Jiang and Y. F. Lu, *Nanotechnology*, 2011, **22**, 165604.
37 Y. Wang, T. Feng, K. Wang, M. Qian, Y. Chen and Z. Sun, *J. Nanomater.*, 2011, **2011**, 935218.
38 A. Laforgue, *J. Power Sources*, 2011, **196**, 559.
39 K. W. Nam, M. G. Kim and K. B. Kim, *J. Phys. Chem. C*, 2007, **111**, 749.
40 D. P. Dubal, D. S. Dhawale, R. R. Salunkhe and C. D. Lokhande, *J. Alloys Compd.*, 2010, **496**, 370.
41 S. Dresselhaus, M. G. Dresselhaus, R. Saito and A. Jorio, *Phys. Rep.*, 2005, **409**, 47.
42 S. B. Ma, K. Y. Ahn, E. S. Lee, K. H. Oh and K. B. Kim, *Carbon*, 2007, **45**, 375.
43 Z. B. Lei, J. Zhang and X. S. Zhao, *J. Mater. Chem.*, 2012, **22**, 153.
44 Y. J. Kang, S. J. Chun, S. S. Lee, B. Y. Kim, J. H. Kim, H. Chung, S. Y. Lee and W. Kim, *ACS Nano*, 2012, **6**, 6400.
45 B. G. Choi, J. Hong, W. H. Hong, P. T. Hammond and H. Park, *ACS Nano*, 2011, **5**, 7205.
46 Y. Xu, Z. Lin, X. Huang, Y. Liu, Y. Huang and X. Duan, *ACS Nano*, 2013, **7**, 4042.
47 L. Peng, X. Peng, B. Liu, C. Wu, Y. Xie and G. Yu, *Nano Lett.*, 2013, **13**, 2151.
48 X. Lu, M. Yu, T. Zhai, G. Wang, S. Xie, T. Liu, C. Liang, Y. Tong and Y. Li, *Nano Lett.*, 2013, **13**, 2628.